Biosensors and Bioelectronics 157 (2020) 112163

Contents lists available at ScienceDirect

Biosensors and Bioelectronics

journal homepage: http://www.elsevier.com/locate/bios

High-density phage particles immobilization in surface-modified bacterial cellulose for ultra-sensitive and selective electrochemical detection of *Staphylococcus aureus*

Umer Farooq [a,1], Muhammad Wajid Ullah [b,1], Qiaoli Yang [a], Ayesha Aziz [a], Jingjing Xu [a], Lei Zhou [a], Shenqi Wang [a,*]

[a] Advanced Biomaterials & Tissue Engineering Centre, Huazhong University of Science and Technology, Wuhan, 430074, PR China
[b] Department of Biomedical Engineering, Huazhong University of Science and Technology, Wuhan, 430074, PR China

ARTICLE INFO

Keywords:
Bacterial cellulose
High-density phage immobilization
Electrochemical biosensor
Sensitivity and selectivity
Live/dead cell discrimination
Staphylococcus aureus detection

ABSTRACT

The routinely used enzymes, antibodies, and nucleic acids-based biosensors for detection of *Staphylococcus aureus* are often overwhelmed by limited selectivity, sensitivity, high cost, and inability to discriminate between live/dead cells. This necessitates the development of an ultra-sensitive, stable, and selective electrochemical biosensor capable of discriminating live *S. aureus* in a mixture of live/dead cells in food samples. The current study reports the development of an electrochemical biosensor through the immobilization of bacteriophage in surface-modified bacterial cellulose (BC) matrix. BC being highly porous and fibrous, offers a high surface area for the impregnation of carboxylated multiwalled carbon nanotubes (c-MWCNTs) and allows high-density phage immobilization. Surface modification of BC/c-MWCNTs with polyethyleneimine (PEI) provides a positive charge that facilitates oriented phage immobilization. FE-SEM and FT-IR analyses confirmed the development of BC/c-MWCNTs-PEI-phage bio-interface. Confocal microscopy analysis showed 11.7 ± 1.2 phage particles·μm^{-2} immobilized in the BC matrix and showed anti-staphylococcal activity by producing clear lytic zone and reduced bacterial growth. Differential pulse voltammetry (DPV) analysis detected 3 CFU·mL^{-1} and 5 CFU·mL^{-1} of *S. aureus* in phosphate buffer saline (PBS) and milk, respectively, within 30 min at neutral pH and showed stability over 6-weeks at 4 °C. The biosensor showed high specificity for *S. aureus*, both in pure and mixed cultures of non-host bacteria, and effectively discriminated live *S. aureus* in a mixture of live/dead cells. The developed biosensor represents a simple, sensitive, specific, and accurate tool for early detection of *S. aureus* in food samples.

1. Introduction

Food protection is an alarming issue to the economy and public health where different bacteria such as *Staphylococcus aureus* and other pathogens cause foodborne diseases (Scharff, 2012). *S. aureus* is an enterotoxin producing, hospital-acquired Gram-positive bacterium found in water, air, and skin of humans and animals (Bhardwaj et al., 2016). It causes different kinds of skin infections and food poisoning (Yuan et al., 2014). Therefore, early and selective detection of *S. aureus* in food samples is crucial to guarantee the food safety and minimize the risk of human exposure to possible bacterial threats (Zhao et al., 2014). Among the available bacterial detection approaches, the conventional ones, although reliable, are laborious and time-consuming (Guo et al., 2016). In contrast, the advanced molecular techniques like immunological (enzyme-linked immunosorbent assay-ELISA) (Guo et al., 2016) and nucleic acid-based methods (polymerase chain reaction-PCR) (Järvinen et al., 2009) require only few hours to complete. However, such techniques are typically expensive, need high-tech laboratory set up and skilled experts, and laborious sample preparation procedures, while at the same time, these cannot discriminate between the live/dead bacterial cells (Farooq et al., 2018).

Since last two decades, extensive efforts have been devoted towards the development of different kinds of biosensors such as electrochemical, optical, piezoelectric, gravimetric, and pyroelectric for rapid, sensitive, and specific detection of pathogens and other applications (Asif et al., 2018; Janczuk-Richter et al., 2019; Pourreza et al., 2015).

* Corresponding author.
E-mail address: shenqiwang131@hust.edu.cn (S. Wang).
[1] These authors contributed equally to this work.

https://doi.org/10.1016/j.bios.2020.112163
Received 13 November 2019; Received in revised form 18 March 2020; Accepted 19 March 2020
Available online 22 March 2020

However, the use of expensive and temperature-, pH-, and environment-sensitive probes such as nucleic acid, enzymes, and antibodies limit their real-world and broad-spectrum applications. Furthermore, the purity of such probes may show false-positive results, or their degradation may end in false-negative output (Moghtader et al., 2016). In contrast, the bacteriophages as bio-probe offer high-specificity and selectivity, and capable of discriminating between live/dead cells (Singh et al., 2013; Wu et al., 2016; Zhou et al., 2017). Further, bacteriophages cost-effectively produce high titer and tolerate the variation in pH and temperature of the growth medium (Farooq et al., 2018). The phage-based biosensors eliminate the sophisticated sample preparation (Wu et al., 2016) and have been reported for detection of various bacteria such as *Escherichia coli* (Shabani et al., 2013), *Bacillus cereus* and *Mycobacterium smegmatis* (Yemini et al., 2007), *S. aureus* (Balasubramanian et al., 2007), and *Salmonella typhimurium* (Lakshmanan et al., 2007).

The use of bacteriophages as bio-probes requires their immobilization on an appropriate substrate in a way that their tail preserves the ability to infect the host bacterium (Zhou et al., 2017). Additionally, the phage particles should be immobilized in a high number for improved performance of biosensor. An active immobilization of phages is achieved in a 'tail-up head down' orientation to allow maximum interaction of the phage's tail spikes with the receptor-binding proteins (RBPs) on bacterial cell wall (Richter et al., 2017). This can be achieved through simple physical adsorption (Moghtader et al., 2016), genetic approaches (Tolba et al., 2010), and electrostatic interaction (Richter et al., 2017). Among these, the electrostatic interaction is a sustainable approach (Bhardwaj et al., 2016) where the phage capsid proteins offer a negative charge and form a stable chemical bond with the positively charged substrate, while its tail fibers remain free for bacterial capture. The substrate used for phage immobilization should be inexpensive, non-toxic, offer a humid environment for phage stability, and provide a high surface area for high-density phage immobilization for sensitive detection and improved performance (Arora et al., 2011; Wang et al., 2012). To date, different substrates such as metal oxides (Liana et al., 2016), metals (Janczuk et al., 2017), carbon-based nanomaterials (Yue et al., 2017), and polymers (Janczuk-Richter et al., 2019), have been used for immobilization of bacteriophages in biosensor development. For example, Bhardwaj et al. used a metal-organic framework (MOF) for phage immobilization to develop a photoluminescence biosensor for *S. aureus* detection with a limit of detection up to 31 CFU/mL (Bhardwaj et al., 2017b); however, the photoluminescence biosensors usually suffer from autofluorescence as well as the turbid sample matrix hinder the signaling (Balasubramanian et al., 2007). In the present study, bacterial cellulose (BC) produced by microbial cells (Ullah et al., 2017) and cell-free system (Ullah et al., 2015), was chosen as a substrate for phage immobilization due to its inimitable properties like never-dried nature, ultrafine fibrous and highly porous structure, high surface area, non-toxicity, surface chemistry, high mechanical strength and flexibility, and high liquid holding capacity (Khan et al., 2018; Ullah et al., 2016). It has already been explored as a carrier in drug delivery systems (Li et al., 2018a), enzyme immobilization (Czaja et al., 2006), sensors (Jasim et al., 2017), and as a scaffold in tissue engineering (Ul-Islam et al., 2019), both alone and in the form of composites with other polymers and nanomaterials (Geisel et al., 2016; Khan et al., 2018). However, pristine BC lacks conductive properties (Khan et al., 2015) and bears a net-negative charge on its surface due to the presence of –OH groups. Therefore, in the present study, carboxylated multi-walled carbon nanotube (c-MWCNTs) were added to BC matrix to impart electrical conductivity (Jasim et al., 2017) while polymerization of polyethyleneimine (PEI) along the BC fibers introduced a positive charge on its surface (Zhou et al., 2017). Thus, the PEI-modified BC with incorporated CNTs (i.e., BC/c-MWCNTs-PEI) can serve as a substrate for phage immobilization and can be used as an electrochemical biosensor for detection of current-voltage changes at the interface of BC/c-MWCNTs-PEI and solution (i.e., the electrode–solution interface) by detecting the variations in the conductivity of the medium or at the electrode–solution interface (Li et al., 2018b; Wang et al., 2017). The developed BC/c-MWCNTs-PEI-phage bio-interface was characterized for its structural and chemical features, as well as anti-staphylococcal and lytic activities of immobilized phages. The surface density of phage particles at the bio-interface was determined through confocal microscopic analysis. The electrochemical performance of the bio-interface was determined by cyclic voltammetry (CV) and differential pulse voltammetry (DPV). The highly-stable BC/c-MWCNTs-PEI-phage bio-interface efficiently and selectively detected 3 CFU·mL^{-1} and 5 CFU·mL^{-1} of *S. aureus* in phosphate buffer saline (PBS) and milk, respectively, only within 30 min. Additionally, the biosensor selectively detected *S. aureus* in the presence of non-host bacteria and effectively discriminated live cells in a mixture of live/dead cells. Overall, this study reports the development of a simple, artless, inexpensive, accurate, and efficient phage-specific bacterial detection tool.

2. Materials and methods

2.1. Materials

The following chemical reagents were obtained and used without further processing: agar powder, peptone, tryptone, yeast extract, and premix of Luria-Bertani (LB) (Alfa Aesar, China), sodium chloride, calcium chloride, disodium phosphate, and polyethylene glycol (EMD chemicals, China), citric acid monohydrate, sodium cyanoborohydride, sodium hydroxide, hydrochloric acid, phosphotungstic acid, polyethyleneimine, and glycerol (Sigma-Aldrich, USA). Multiwall carbon nanotubes (XFNANO Inc., China) were carboxylated through acid-treatment.

2.2. Bacterial culture

The phage's host strain *Staphylococcus aureus* (CCTCC AB2013186) and non-host strains, including *S. typhimurium* (CCTCC TA98) and *E. coli* (CCTCC AB20005) were purchased from China Center for Type Culture Collection (China). *Gluconacetobacter xylinum, Klebsiella pneumonia*, *Pseudomonas aeruginosa*, and *Yersinia pseudotuberculosis* were kindly provided by the 3-Bio Lab at the Department of Biomedical Engineering, Huazhong University of Science and Technology (Wuhan, China).

2.3. Phage isolation and propagation

The *S. aureus*-specific lytic phage was isolated from the hospital sewage water following a previously reported protocol (Pallavali et al., 2017) with minor modifications. Briefly, 500 mL of sewage water from the sewage treatment plant of Tongji Hospital (Wuhan, China) was collected and centrifuged at 6000×*g* for 10 min at room temperature to remove the solid particles and debris. The supernatant was filtered using a 0.22 μm syringe-driven filter, and the filtrate was stored at 4 °C. The filtrate was amplified by double-layer agar (DLA) method for isolation and titration of phage. The quantified phage titer was stated in plaque-forming units per milliliter (PFU·mL^{-1}) (**Supplementary information**).

2.4. BC production

BC sheets were produced statically in square containers (15 cm × 15 cm × 7 cm) by incubating the *G. xylinum* in Hestrin and Schramm (HS) growth medium containing glucose 20 g.L^{-1}, yeast extract 5 g.L^{-1}, peptone 5 g.L^{-1}, disodium phosphate 2.7 g.L^{-1}, and citric acid monohydrate 1.15 g.L^{-1}, as reported previously (Khan et al., 2018). The pH of the medium was adjusted to 5 and autoclaved at 15 psi and 121 °C for 30 min. Briefly, few colonies from *G. xylinum* culture plate were inoculated into 100 mL of HS broth in a 250 mL Erlenmeyer flask and shaking incubated at 150 rpm for 24 h at 30 °C. Thereafter, 3–5% (v/v)

from this pre-culture was inoculated into freshly prepared 1 L of HS medium (pH 5) and incubated statically at 30 °C for 7–10 days. The produced BC sheet was harvested and treated with 0.3 M NaOH for 15 min at 15 psi at 121 °C to disrupt and dissolve the cell debris, as reported previously (Ul-Islam et al., 2013). Thereafter, the BC sheet was washed several times with deionized distilled water until the pH became neutral. The washed BC sheet was cut into small pieces (2 cm × 5 cm) and stored in distilled water at 4 °C for further use.

2.5. Development of BC/c-MWCNTs-PEI composites

The as-received MWCNTs were carboxylated through acid-treatment, following a previously reported protocol (Lv et al., 2018). Briefly, the BC pieces were suspended in 0.1, 0.5, and 1 wt% c-MWCNTs suspension, prepared in distilled water and sonicated for 1 h to prepare the BC/c-MWCNTs(I), BC/c-MWCNTs(II), and BC/c-MWCNTs(III) nanocomposites, respectively. The prepared nanocomposites were washed with distilled water to remove the freely adsorbed c-MWCNTs on the BC surface. Thereafter, the BC/c-MWCNTs nanocomposites were polymerized with PEI following a previously reported protocol (Jin et al., 2017) with minor modifications. Briefly, the nanocomposites were suspended in 5 wt% PEI solution, and the pH was adjusted to 7 using 0.1 M HCl. Further, 0.21 wt% sodium cyanoborohydride was added to the reaction mixture to accelerate the polymerization process carried out by sonication for 1 h. The prepred composites were referred to as BC/c-MWCNTs(I)-PEI, BC/c-MWCNTs(II)-PEI, and BC/c-MWCNTs (III)-PEI, according to the concentrations of c-MWCNTs.

2.6. Phage immobilization

The different BC/c-MWCNTs(I-III)-PEI composites were separately suspended in already propagated phage solution at a titer of 1×10^9 PFU·mL^{-1} and shaking incubated at 120 rpm for 6 h. The sheets were then washed with water through shaking while changing the water after each hour for a total of 6 h. Finally, the sheets were collected and named as BC/c-MWCNTs(I)-PEI-phage, BC/c-MWCNTs(II)-PEI-phage, and BC/c-MWCNTs(III)-PEI-phage. All composites were freeze-dried and stored at 4 °C for further analysis.

2.7. Morphological, and functional groups characterization

The structural morphologies of pristine BC, c-MWCNTs, and different composites before and after the phage immobilization were observed under field emission scanning electron microscope (Nova Nano FE-SEM 450, Dutch FEI). Prior to observation, the samples were fixed on aluminum stubs, coated with a 5 nm layer of gold, and observed using FE-SEM operated at 30 kV. The chemical structures of pristine BC, c-MWCNTs, and different composites were determined through Fourier transform infrared spectroscopy (FT-IR, VERTEX 70 German Bruker). The FT-IR data were collected at a resolution of 4 cm^{-1} with 16 scans per spectrum in the wavelength region between 4000 and 400 cm^{-1} at room temperature.

2.8. Plaque assay of immobilized phages

To perform the plaque assay, a 100 μL overnight culture of *S. aureus* was mixed with 4 mL of LB top agar tubes (0.5% agar) maintained at 50 °C and spread onto LB bottom agar plates (1.5% agar). After solidification, the phage treated BC, BC/c-MWCNTs(I-III), BC/c-MWCNTs(I-III)-PEI films were carefully placed in the middle of *S. aureus*-cultured top agar plates. Here, the pristine BC, BC/c-MWCNTs(I-III), and BC/c-MWCNTs(I-III)-PEI films were used as control and placed on the *S. aureus*-cultured top agar plates. Furthermore, the phage-treated BC, BC/c-MWCNTs(I-III), BC/c-MWCNTs(I-III)-PEI films were sonicated for 15 min and placed on the *S. aureus*-cultured top agar plates. All plates were overnight incubated at 37 °C and observed for plaques formation around the edges of the composite films.

2.9. Cell-lysis efficiency of immobilized phages

For cell lysis efficiency of immobilized phages, a 30 mL of *S. aureus* culture was transferred to the separate flasks and pre-incubated at 37 °C until its OD_{600} reached 0.1. The flasks were then inoculated with the films of phage-treated BC, BC/c-MWCNTs(I-III), and BC/c-MWCNTs(I-III)-PEI, and shaking incubated (150 rpm) at 37 °C. The OD_{600} was determined after every hour for a total of 11 h of infection. For comparison, the pure *S. aureus* culture was used as the negative control, while the *S. aureus* culture inoculated with 500 μL phage was used as a positive control. Finally, the growth curves were obtained and compared to determine the cell-lysis efficiency of immobilized phages in the BC/c-MWCNTs-PEI bio-interface.

2.10. Confocal microscopy

The immobilized phage particles on the developed BC/c-MWCNTs-PEI bio-interface was observed through confocal microscopy. Briefly, the immobilized phages on 1 × 1 cm composite films were stained with 10 μL of diluted 15 × SYBR gold (a fluorescent nucleic acid stain, Life Technologies, Carlsbad, USA) solution for 30 min at room temperature in the dark. The excess stain was washed with PBS, and the films were placed on the glass slides (Wang et al., 2016a). Before placing the cover slide, a drop of the antifading agent was added and observed using a confocal microscope (Olympus FV1000) with an oil immersion lens of 60x. The images were processed with ImageJ software (ImageJ 1.52n, NIH-USA) to determine the density of the immobilized phage particles.

2.11. Electrochemical characterization

The electrochemical performance of as-prepared BC/c-MWCNTs(I-III)-PEI-phage bio-interface was determined through cyclic voltammetry (CV) and differential pulse voltammetry (DPV) by using the differently developed composites as the working electrodes. Briefly, the electrodes were cut into 0.5 cm × 1 cm pieces, and CV and DPV were performed using the CHI660E electrochemical workstation (Shanghai Chenhua Instruments Co. Ltd., China). A conventional three-electrode cell (a Pt wire - auxiliary electrode, Ag/AgCl - reference electrode, and a BC/phage-based working electrode) was used for electrochemical characterization. All measurements were performed at 25 ± 2 °C in 10 mL voltammetry cell containing electro-catalytic solution (5 mM 1:1 $K_3Fe(CN)_6$ and $K_4Fe(CN)_6$ with 0.1 M KCl) for electrode optimization unless otherwise stated. The DPV-based current response was used to measure the electrical signal generated during the *S. aureus* capture and lysis to perform the electrochemical detection in PBS (pH 7 with 0.05 mM 1:1 $K_{3/4}Fe(CN)_6$).

2.12. Optimization of biosensor

The response time of biosensor was determined by analyzing the current response over 10–60 min of incubation while taking the reading after every 5 min. Briefly, the developed BC/c-MWCNTs-PEI-phage electrode was placed in 10 mL PBS (pH 7 with 0.05 mM 1:1 $K_{3/4}Fe(CN)_6$) containing 6×10^3 CFU·mL^{-1} of *S. aureus* (random and constant). The DPV-based current response was determined between 10 and 60 min after every 5 min. The sensitivity of biosensor was also determined by placing the electrode in PBS solution at pH 4–10 containing 6×10^3 CFU·mL^{-1} of *S. aureus* (random and constant). The electrode was incubated for the optimized time, and the current was recorded to obtain the pH-dependent current response variations. After the optimization of response time and pH, the developed biosensor was employed for the detection of *S. aureus* in PBS. The response of the electrode was recorded by incubating it in PBS inoculated with 3×10^0 to 3×10^7 CFU·mL^{-1} of *S. aureus*. The variation in current response at different concentrations of

S. aureus was recorded.

2.13. Selectivity, accuracy, and live/dead cell discrimination

The selectivity of the developed biosensor was determined against *S. aureus* and other non-specific bacteria like *E. coli, S. typhi, P. aeruginosa,* and *Y. pseudotuberculosis*. Briefly, the different bacteria were freshly grown in their respective media for 11 h with ~10^6 CFU·mL^{-1}, followed by centrifugation at 5000×*g* for 3 min. The pelleted cells were re-suspended in 10 mL of PBS (pH 7 with 0.05 mM 1:1 $K_{3/4}Fe(CN)_6$). The biosensor response was recorded for *S. aureus* and other non-specific bacteria, with PBS as a positive control. The assay was also performed for a mixture of all non-specific bacteria and *S. aureus*. The practical application of the developed BC/phage-based biosensor was determined in real food samples: i.e., 20% (v/v) milk spiked in PBS with concentrations of 5 × 10^0 to 5 × 10^6 CFU·mL^{-1} of *S. aureus*.

The accuracy of the developed BC/phage-based biosensor was determined by comparatively quantifying the number of *S. aureus* in PBS and milk samples by the BC/c-MWCNTs-PEI-phage biosensor and conventional culturing and plate count methods. Briefly, PBS and milk samples with known concentrations of *S. aureus*, i.e., 3 × 10^3 and 5.2 × 10^3 CFU·mL^{-1}, respectively, were prepared, and the accuracy was evaluated by determining the % recovery. Further, the ability of BC/c-MWCNTs-PEI-phage biosensor to discriminate live bacterial cells in a mixture of live/dead cells by measuring the DPV current response in ~10^6 CFU·mL^{-1} of live cells and comparable amounts of dead cells obtained by heating *S. aureus* culture at 100 °C for 10 min.

3. Results and discussion

The *S. aureus*-specific phage was successfully isolated from the hospital sewage by double-layer agar (DLA) method, as shown by the clear lysis plaques produced by the phages in the lawn of the host bacterial cells (Fig. S1). TEM micrographs showed that the isolated phage particles were tailed and possessed a hexagonal capsid of ~100 nm (Fig. S2). The isolated phage particles showed high lytic specificity towards *S. aureus* (Table S1). As the final goal of the present study was to develop a BC/phage-based bio-interface for *S. aureus* detection, the carboxylated MWCNTs (Fig. S3) were impregnated into the matrix of produced BC sheets (Fig. S4) through simple *ex-situ* blending. In the BC-c-MWCNTs nanocomposite, the ultra-fibrous and highly porous network structure of BC allowed the impregnation of c-MWCNTs and their adhesion to the cellulose fibers, thus imparting the conductive properties to BC, as reported previously (Lv et al., 2016; Yoon et al., 2006). Further, the BC fibers were partially modified with PEI to impart a positive charge (Scheme 1). Finally, the phage particles were immobilized in the BC matrix through electrostatic interaction between the PEI-modified positively charged BC fibers that interact with the negative charges on the phage head. Thus, polymerization of PEI, an amine rich poly-cation, worked as a reducing agent during the synthesis of BC/c-MWCNTs-PEI composite (Zhou et al., 2017) as well as a linker for the binding of anionic phage head (Goeller and Riley, 2007). The possible chemical interaction during the PEI polymerization could be the hydrogen bonding between the amine groups arising from PEI with the –COOH groups of c-MWCNTs and the –OH groups of BC (Zhang et al., 2010). Some amino acid sequences that arise from the phage head proteins like –COOH and C–C groups potentially favor the chemical interactions with the PEI-functionalized BC/c-MWCNTs composite (Goeller and Riley, 2007). This suggests that polymerization of PEI along the BC fibers could favor the oriented phage immobilization by interacting with the anionic phage capsid while exposing the positively charged tail-spikes for bacterial capture, whereas the highly porous structure of BC favors the immobilization of maximum phage particles. The entire fabrication and sensing application of the developed BC-c-MWCNTs-PEI-phage bio--interface is illustrated in Scheme 1.

3.1. Structural morphology of BC/c-MWCNTs-PEI-phage bio-interface

The diameter distribution, and micro- and nano-morphological structures of pristine BC, BC/c-MWCNTs, BC/c-MWCNTs-PEI, and BC/c-MWCNTs-PEI-phage composite membranes were determined from the FE-SEM micrographs (Fig. 1A–E). FE-SEM micrographs showed that pristine BC possessed fine fibrillar architecture comprised of a porous 3D web-like arrangement of fibrils which are loosely arranged and range in size from a few micrometers to >1 μm in length (Fig. 1A). These observations are in accordance with the previous reports (Ul-Islam et al., 2014; Zhang et al., 2010). Further, the diameter of the fibrils was ranged between 10 and 75 nm with an average diameter of about 40 nm. This highly porous and 3D web-like arrangement of cellulose fibrils allowed the impregnation of c-MWCNTs into the BC matrix. Fig. 1B shows the

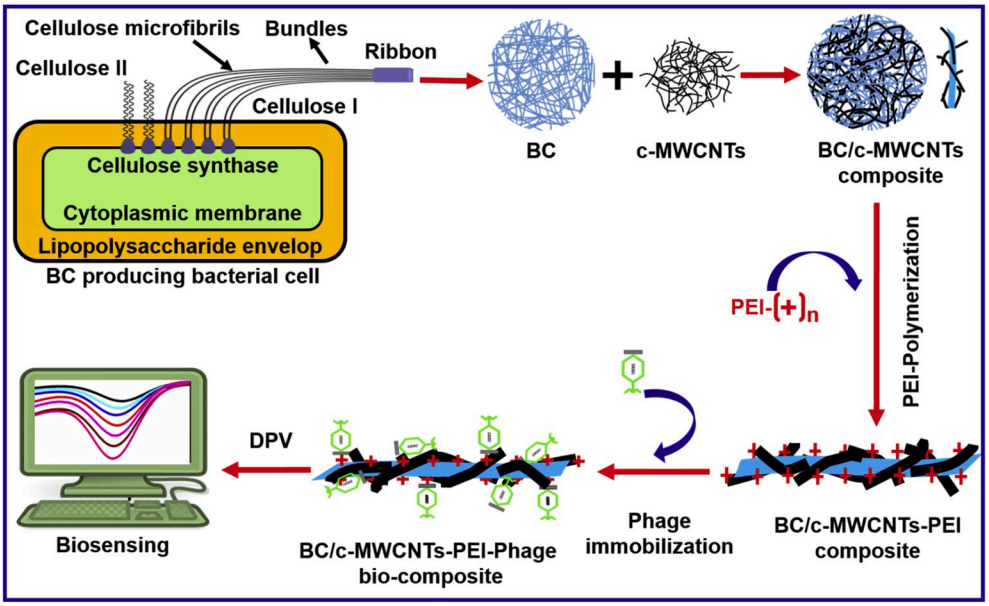

Scheme 1. Schematic representation of BC production, incorporation of c-MWCNTs into its matrix, its cationic modification with PEI, and immobilization of phages in the PEI-modified BC fibers, and application of the developed bio-interface in the development of DPV-based electrochemical bacterial detection.

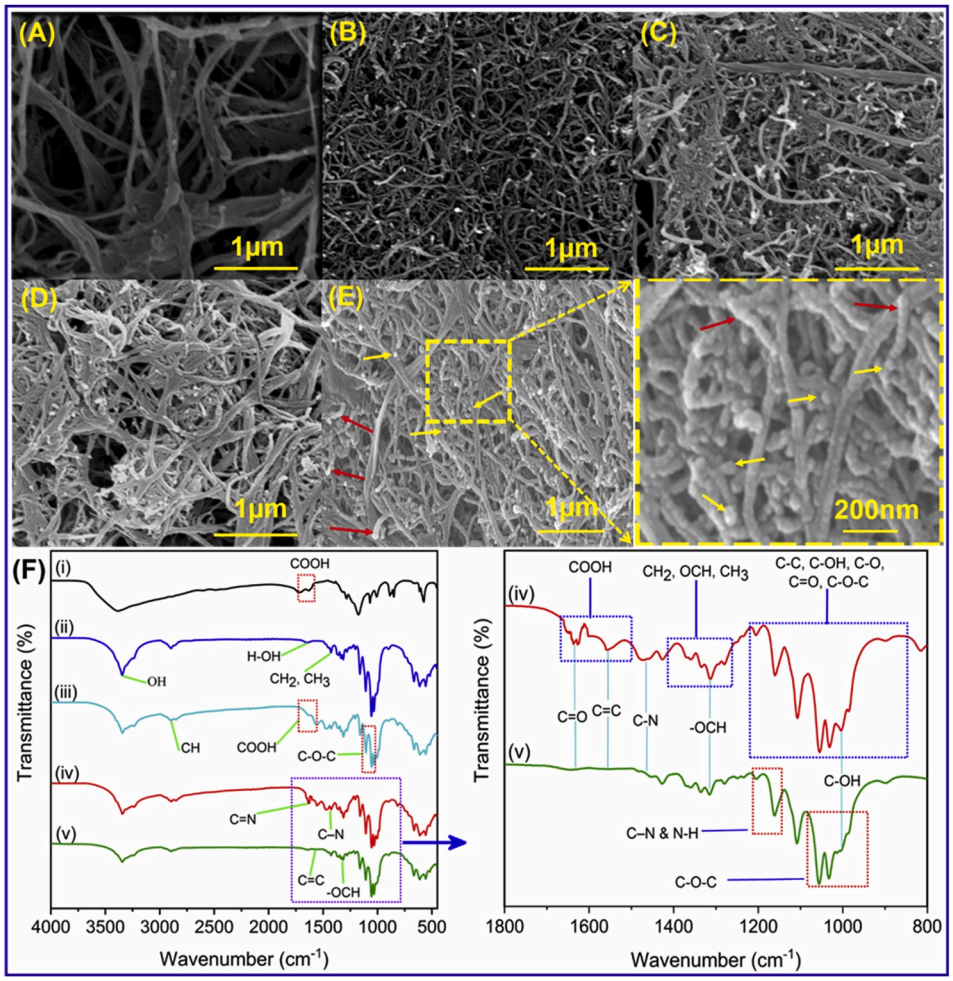

Fig. 1. Morphological and chemical structure characterization of pristine BC and BC/c-MWCNTs-PEI-phage composite. (A–E) FE-SEM observation of (A) pristine BC, (B) carboxylated MWCNTs, (C) BC/c-MWCNTs, (D) BC/c-MWCNTs-PEI, and (E) BC/c-MWCNTs-PEI-phage. The selected magnified area of BC/c-MWCNTs-PEI-phage in (E) is also shown where the red arrows represent the c-MWCNTs, while the yellow arrows denote the phage particles. (F) Comparative FT-IR analysis of (i) c-MWCNTs, (ii) pristine BC, (iii) BC/c-MWCNTs, (iv) BC/c-MWCNTs-PEI, and (v) BC/c-MWCNTs-PEI-phage. The selected magnified area in (F) shows the FT-IR-finger print of BC/c-MWCNTs-PEI and BC/c-MWCNTs-PEI-phage ranging in the wavelength between 1800 and 800 cm^{-1}. (For interpretation of the references to colour in this figure legend, the reader is referred to the Web version of this article.)

FE-SEM micrograph of c-MWCNTs and their size distribution with a diameter ranging between 10 and 20 nm, which are comparable with the diameter of the non-carboxylated MWCNTs as-received from the manufacturer, indicating that carboxylation did not affect their diameter. The c-MWCNTs were successfully impregnated into the BC matrix and formed the BC/c-MWCNTs nanocomposite (Fig. 1C). In the BC/c-MWCNTs nanocomposite, the adhesion of nanotubes to the cellulose fibers could be due to their adsorption into the matrix (Lv et al., 2016; Yoon et al., 2006).

Polymerization of amine-rich PEI worked both as a reducing agent in the synthesis of BC/c-MWCNTs (Zhou et al., 2017) and as a linking molecule for anionic phage-head anchorage. Thus, the positively charged BC/c-MWCNTs-PEI composite was used for the oriented immobilization of phage. The FE-SEM micrograph of BC/c-MWCNTs composite before and after the PEI cationic polymerization clearly showed different structural morphologies with some clumps of c-MWCNTs and many mesoporous structures produced after PEI polymerization (Fig. 1D). These observations are in accordance with a previous study (Wang et al., 2015). These observations further suggest that the synthesis of BC/c-MWCNTs-PEI composite involves the formation of hydrogen bonding between the amine group of PEI with the –OH group of BC or the –COOH group of c-MWCNTs (Zhang et al., 2010). This nano-porous conductive architecture and cationic surface charge of the fibers provided a suitable environment for anionic phage head attachment as well as high surface area for maximum immobilization of phage particles. To attain a maximum bacterial capture efficiency of the phage particles, these should be immobilized in such a way that the anionic phage head is bonded to the substrate while the tail-spikes are exposed. The oriented immobilization of "tail up-heads down" allows the recognition of bacterial cells that bind to the bacterial cell wall by the free tail fibers (Zhou et al., 2017). Fig. 1E shows the attachment of phage particles to the BC/c-MWCNTs-PEI composite, where the red arrows represent the c-MWCNTs while the yellow arrows denote the immobilized phage particles.

3.2. Chemical properties of BC/c-MWCNTs-PEI-phage bio-interface

FT-IR analysis was carried out to confirm the carboxylation of MWCNTs and their impregnation into the BC matrix as well as polymerization of PEI along the BC fibers and immobilization of phage particles in the BC/c-MWCNTs-PEI nanocomposite; the combined spectra are shown in Fig. 1F. The curve (i) for c-MWCNTs shows the characteristic peaks for carboxylate groups and carboxylic acid at 1565 cm^{-1} and 1714 cm^{-1}, respectively. Such peaks are produced during the acid-treatment (Chen et al., 2009). A broad peak centered at 3398 cm^{-1} was ascribed to –OH group. The curve (ii) represents the typical cellulose curve containing the characteristic peak for –OH at 3343 cm^{-1}. Further, the peaks for stretching vibration appeared at 3500 cm^{-1} and 3000 cm^{-1}, which are involved in the inter- and intra-chain hydrogen bonding within the cellulose units (Yue et al., 2015). The bands due to the symmetric and asymmetric stretching vibrations of C–H groups appeared at 2902 cm^{-1}. The peaks related to CH_2 and CH_3 deformation appeared between 1400 and 1370 cm^{-1}, while the peak due to C–O–C deformation vibration and C–O stretching vibration appeared at 1113 and 1033 cm^{-1}, respectively. These observations are in accordance with the previous reports (Maria Manzine Costa et al., 2012;

Szymańska-Chargot et al., 2011). The curve (iii) represents the FT-IR spectrum of BC/c-MWCNTs nanocomposite, which showed a broadening of the peak for carboxylate group and shifting of the peak for carboxylic acid, indicating the incorporation of c-MWCNTs into the BC matrix. Many amine groups present on the PEI react with the available aldehyde groups and form the C═N bond; nevertheless, this reaction is reversible, and the resulting C═N bonding can be back-hydrolyzed to di-aldehyde cellulose by the actions of dilute alkalis or dilute acids (Huang et al., 2018). To prevent this reversible reaction, the addition of sodium cyanoborohydride ($NaBH_3CN$) convert the C═N bond into the C–N bond and form the PEI-modified BC/c-MWCNTs-PEI composite. The curve (iv) shows a decrease in the peak intensity at 3343 cm^{-1} for –OH group, demonstrating the cationic PEI polymerization on the BC/c-MWCNTs nanocomposite. Further, the intensified peak at 1626 cm^{-1} was due to the C–N and C═N stretching, demonstrating the successful polymerization of PEI on BC/c-MWCNTs nanocomposite, as reported previously (Jin et al., 2017). In addition, the intensification of the peak at 1565 cm^{-1} could be due to the NH_2 and N–H wagging of PEI (Bhardwaj et al., 2016). The curve (v) for BC/c-MWCNTs-PEI-phage shows a higher transmittance peak at 2902 cm^{-1} as compared to the BC/c-MWCNTs–PEI composite.

The fingerprint area after the phage immobilization in the BC/c-MWCNTs–PEI nanocomposite lied in the range between 1800 and 800 cm^{-1}, which is shown as a magnified image. In curve (iv), the characteristic band for the amide I plane C═O stretching vibration appeared at 1645 cm^{-1} while that for the amide II plane C–N stretching and N–H bending appeared at 1565 cm^{-1}, which is in agreement with a previous report (Dong et al., 2013). The absence of a wide peak in the region 1642-1535 cm^{-1} in the phage-immobilized composite could be attributed to the imine bond formation (Preisner et al., 2010). The peak at 1474 cm^{-1} due to CH_2 bending/scissoring and CH_3 asymmetric bending disappeared in the phage-immobilized composite, while another peak appeared at 1425 cm^{-1} due to the C–N stretching in the phage-immobilized composite. Furthermore, the low-intensity peak at 1314 cm^{-1} could be due to the rocking vibration of CH_2 while the sharpening of the peak in the range between 1240 and 1188 cm^{-1} could be due to the N–H in-plane bending and C–N stretching. These peaks might have appeared from the interaction of phage head proteins, as reported elsewhere (Goeller and Riley, 2007; Jarvis and Goodacre, 2004; Preisner et al., 2010). The low-intensity bands between 1030 and 1005 cm^{-1} could be attributed to the C–O–C, C–C, and C–OH bonding to phage head proteins (Jarvis and Goodacre, 2004).

The characteristic FT-IR spectra in Fig. 1F shows the chemical interaction of the phage head proteins with the different functional groups of the BC/c-MWCNTs-PEI composite. The variations in the band intensity and position for C–C stretching, CH_2 stretching, C═O stretching, CH_2 wagging, C–OH bending, C–O–C stretching, and amide N–H bending suggest the possible involvement of different functional groups of the phage head proteins during the phage immobilization, which are in accordance with the available literature (Dong et al., 2013). Further, the different functional groups such as –COOH and C–C arising from the aspartate and glutamate of phage head proteins could also interact with the PEI-functionalized BC/c-MWCNTs composite (Goeller and Riley, 2007). Although the phage head possesses a net negative charge while its surface chemistry is very little known (Anany et al., 2011), the endogenous amino acids such as glutamate, aspartate, cysteine, lysine, and tyrosine present on the phage head protein favor the basic conjugation schemes for attachments (Hosseinidoust et al., 2014). The negatively charged –COOH arising from these amino acids interact with the positively charged amines of PEI, and thus, an electrostatic interaction is established between the phage head amino acids and amines of PEI (Archer and Liu, 2009).

3.3. The anti-staphylococcal activity of immobilized phages

The anti-staphylococcal activity of the immobilized phages in the BC/c-MWCNTs-PEI composite was determined through the disk-diffusion method and infection dynamics. The immobilization of phage particles to any surface does not guarantee their antibacterial activity or improved bacterial recognition; rather, these should preserve their active integrity of recognition proteins through proper orientation and attachment (Hosseinidoust et al., 2014). The efficiency of immobilized phages on pristine BC and BC-based composites to recognize and infect the *S. aureus* was determined through plaque assays. The result showed that in the absence of phages, the pristine BC, BC/c-MWCNTs, and BC/c-MWCNTs-PEI films did not show bacterial lysis, suggesting that these materials are non-toxic towards *S. aureus* (Fig. 2A–G). In contrast, the phage-immobilized films, including BC/phage, BC/c-MWCNTs/phage, and BC/c-MWCNTs-PEI-phage showed the formation of clear plaques around the films (Fig. 2H-N). Specifically, the pristine BC and BC/c-MWCNTs films showed the immobilization of little amount of phage particles, possibly through physical absorption, that resulted in the formation of small plaques. In contrast, the BC/c-MWCNTs-PEI films showed better lytic activity, suggesting an oriented and a greater number of active phages immobilization. The plaque assay was also performed for phage-immobilized BC and BC composite film after sonication for 15 min to confirm the immobilization of phages with the substrate and to detach the loosely attached phage particles. The results showed that no plaques were formed by the BC/phage and BC/-MWCNTs films (Fig. 2O–R), indicating an unstable binding by simple surface adsorption of phage particles, and their subsequent detachment during the sonication. In contrast, the lysis zones were produced by the BC/c-MWCNTs-PEI-phage composites films (Fig. 2S-U), indicating a stable immobilization of phage particles, possibly through electrostatic interaction between the negatively charged phage particles and positively charged PEI-polymerized along the BC fibers.

To further evaluate the recognition and capturing of *S. aureus* by the immobilized phages, the infection of *S. aureus* cells was initiated by immersing the phage-treated films in 30 mL of LB culture with a density of 1×10^8 CFU·mL^{-1} and OD_{600} were determined after each hour. The initial multiplicity of infection (MOI-number of PFU·mL^{-1}/CFU·mL^{-1}) was determined by comparing the results of pure and phage-infected *S. aureus* cultures. The dynamics of infections are typically decided by the initial MOI, while the number of actively immobilized phages on the film influences the infection dynamics. The results showed that the non-infected *S. aureus* cell reached a static period after 9 h (Fig. 3A). The infection was initiated with the initial MOI 0.1 of phage suspension that completed the lysis of *S. aureus* in 3 h. The infection initiated by the free phage particles with MOI 0.1 was just followed by the BC/c-MWCNTs(I-III)-PEI-phage films (Fig. 3A). The fact of close infection dynamics of phages immobilized on PEI modified cationic films to infection dynamics of free phages indicated a sufficient, active, and oriented immobilization of phages, which can recognize and bind to maximum host *S. aureus*. The infections caused by the BC/phage, BC/c-MWCNTs(I-III)/phage films was comparable with the negative control, i.e., *S. aureus* culture (Fig. 3A). These results suggest that the BC/phage and BC/c-MWCNTs(I-III)/phage films possess very limited active phage particles for bacterial recognition. In contrast, the BC/c-MWCNTs(II)/phage film showed an improved initial MOI as compared to the BC/c-MWCNTs(I)/phage and BC/c-MWCNTs(III)/phage films. Similarly, the BC/c-MWCNTs(II)-PEI-phage film showed higher initial MOI as compared to the BC/c-MWCNTs(I)-PEI-phage and BC/c-MWCNTs(III)-PEI-phage. These observations indicate that the phages were completely entrapped in the BC fibers when 0.1 wt% c-MWCNTs, while the surface topology of the BC membrane might be completely covered by the carbon nanotubes when 1 wt% c-MWCNTs were used in the composite preparation. It was presumed that BC retained its porous morphology when 0.5 w.% c-MWCNTs were used in the composite preparation that neither supported the entrapment of phage particles nor hindered their attachment. Interestingly, the PEI-modified cationic BC films (i.e., BC/c-MWCNTs-PEI-phage) showed the highest anti-staphylococcal and lytic

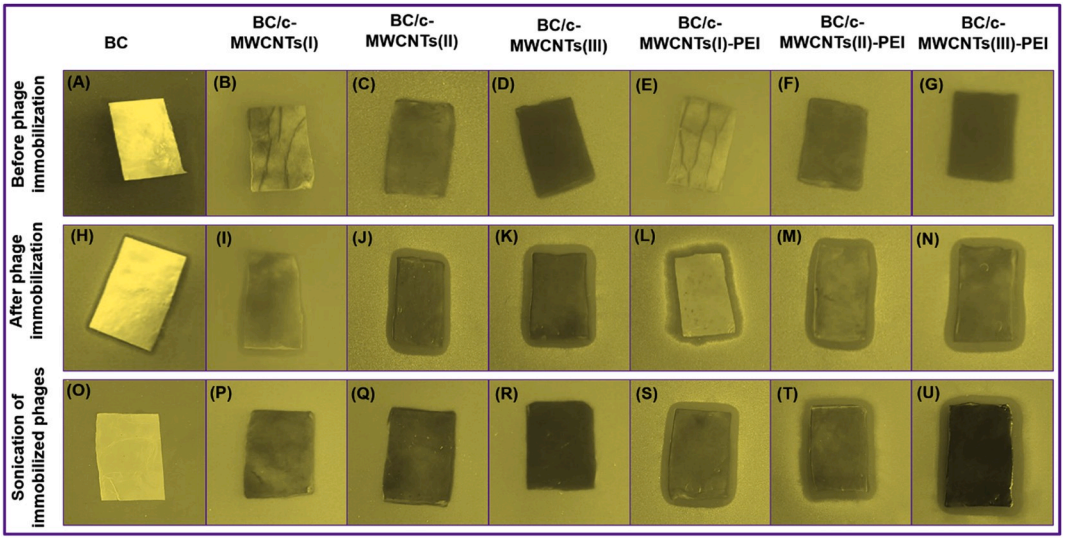

Fig. 2. The anti-staphylococcal activity of pristine BC and BC/c-MWCNTs, BC/c-MWCNTs-PEI, and BC/c-MWCNTs-PEI-phage films determined through the disc diffusion method. (A–G) pristine BC, BC/c-MWCNTs(I-III), and BC/c-MWCNTs(I-III)-PEI films showing no anti-staphylococcal activity without phage immobilization. (H–N) BC/phage, BC/c-MWCNTs(I-III)/phage, and BC/c-MWCNTs(I-III)-PEI-phage films showing obvious anti-staphylococcal activity after phage immobilization. (O–R) The sonicated BC/phage and BC/c-MWCNTs(I-III)/phage did not show anti-staphylococcal activity, representing unstable immobilization of phages. (S–U) The sonicated BC/c-MWCNTs(I-III)-PEI-phage showed obvious anti-staphylococcal activity, representing stable immobilization of phages.

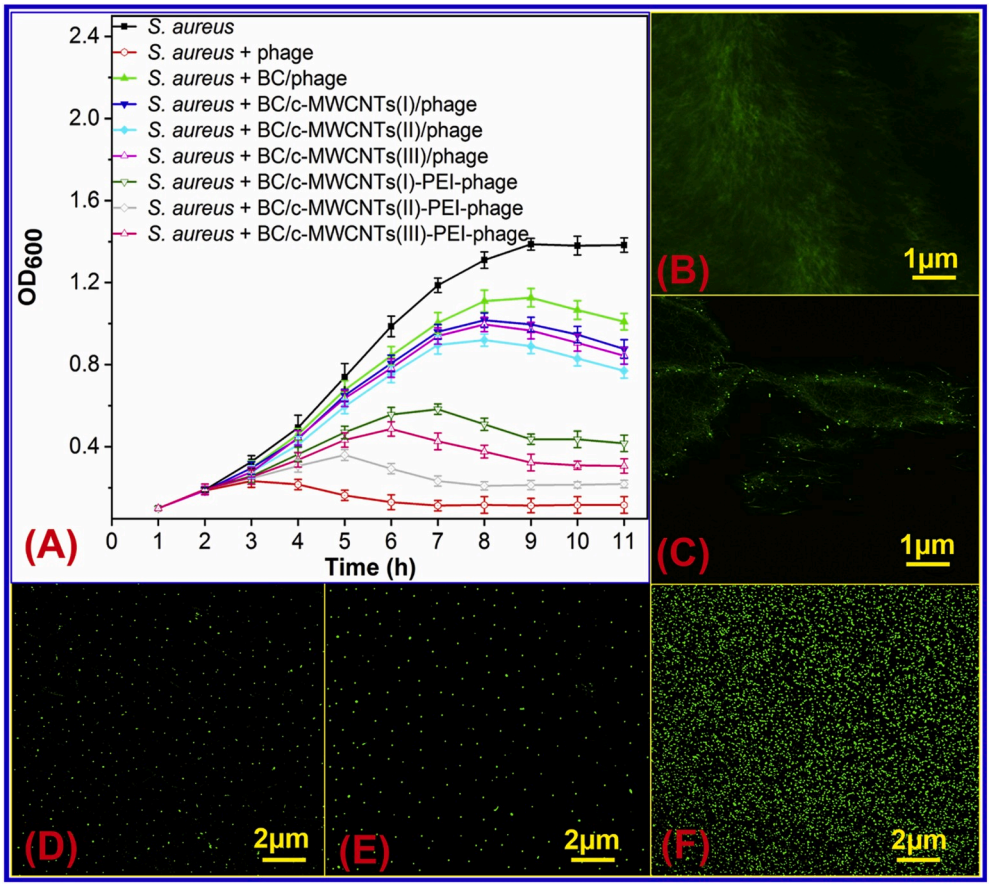

Fig. 3. The anti-staphylococcal activity of immobilized phages determined as a measurement of optical density (OD_{600}) with increasing incubation time and morphology observation of phage particles and their density determined through confocal microscopic observation. (A) represent the growth reduction curves in term of optical densities of pure *S. aureus* culture, and *S. aureus* cultures infected with free phages and phages immobilized on BC, BC/c-MWCNTs(I-III), and BC/c-MWCNTs(I-III)-PEI composites, by recording the OD_{600} at the interval of 1 h and total for 11 h. The standard deviations of triplicate measurements are indicated by the error bars, analyzed by the Origin Pro Software. (B–F) Shows the morphology and densities of immobilized phages by confocal microscopy, where (B) indicate BC without phage immobilization and (C) represents the in-focus morphology observation of immobilized phage particles on BC. (D–F) Show the densities of immobilized stained phage particles (in-focus), while BC and c-MWCNTs were kept out-of-focus, where (D) phage immobilized in pristine BC, (E) phage immobilized in BC/c-MWCNTs composite, and (F) phage immobilized in BC/c-MWCNTs-PEI composite.

activities during the plaque assays and infection dynamics analyses, respectively. During plaque assay, the PEI modified BC composites retained the lytic activity of phages even after 15 min of sonication, suggesting a stable phage immobilization. Thus, it can be concluded that the PEI polymerization of cellulose fibers favored the active immobilization of phages with capsid residues or, at least, with residues that do not hamper the tail proteins involved in bacterial recognition.

3.4. Confocal microscopic observation of BC/c-MWCNTs-PEI-phage bio-interface

The density and distribution of immobilized phage particles both on the surface of BC and impregnated into the BC matrix are the essential characteristics that ultimately influence the antibacterial activity of the film. The density and distribution of phage particles in the developed BC/c-MWCNTs-PEI-phage composite were observed through a confocal microscope, and the results are shown in Fig. 3B–F. The confocal image of the pristine BC revealed the expected fibrous structure of BC (Fig. 3B). To study the morphology of BC fibers and the phages together, the in-focus image of BC with immobilized phages, both on the surface and within the matrix, is shown in Fig. 3C which shows the successful immobilization of phages along the cellulose fibers. Fig. 3D–F shows the densities of immobilized phages on composites like, BC/phage, BC/c-MWCNTs/phage, and BC/c-MWCNTs-PEI-phage, where only the phage particles were focused while the BC and c-MWCNTs were kept out-of-focus, by using the special focusing function in the confocal microscope (Zhou et al., 2017). The results did not show much difference in the densities of the immobilized phages in BC/phage (Fig. 3D) and BC/c-MWCNTs/phage (Fig. 3E), whereas a greater density of immobilized phage particles was observed in BC/c-MWCNTs-PEI-phage (Fig. 3F). The calculated densities by ImageJ software were 1.9 ± 0.2 phage particles·μm^{-2}, 2.1 ± 0.2 phage particles·μm^{-2}, and 11.7 ± 1.2 phage particles·μm^{-2} for BC/phage, BC/c-MWCNTs/phage, and BC/c-MWCNTs-PEI-phage-based composites, respectively. This high immobilized phage particles density on BC/c-MWCNTs-PEI-phage composites as compared to gold (3.67 ± 1.1 phage particles·μm^{-2}) (Singh et al., 2009) and modified poly(hydroxy alkenoate) (4.24 ± 0.84 phage particles·μm^{-2}) (Wang et al., 2016a) could be attributed to the porosity and high surface area of BC. These results indicated that polymerization of PEI along BC fibers supported the immobilization of phage particles, possibly through electrostatic interaction.

3.5. Optimization of the electrode by electrochemical characterization

The electrochemical characterization of the developed BC/c-MWCNTs-PEI-phage-based electrode is presented in Fig. 4. The CV curves of BC-based composites concerning different concentrations of carbon nanotubes are shown in Fig. 4A–C. The CV curves showed that, regardless of different concentrations of c-MWCNTs, the current response of the BC/c-MWCNTs composites increased from zero as compared to pristine BC, followed by an increase in the current response upon polymerization of PEI, while the BC/c-MWCNTs-PEI-phage showed the highest current response. These results demonstrate that the addition of PEI increased the electron transfer between the BC/c-MWCNTs surface and the solution (Kumar et al., 2016). Similarly, the immobilization of phage particles further increased the electron transfer

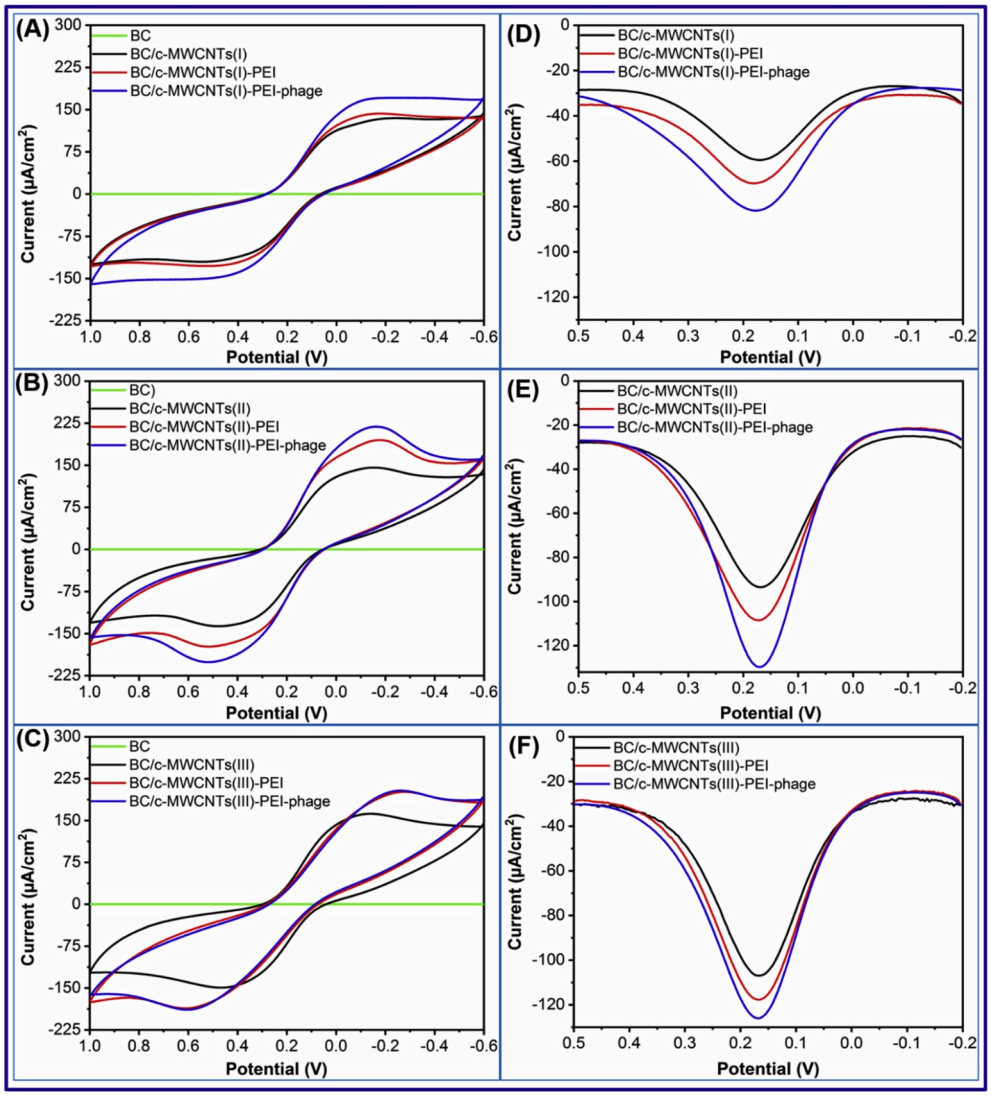

Fig. 4. Electrochemical characterization of BC/c-MWCNTs(I-III), BC/c-MWCNTs(I-III)-PEI, and BC/c-MWCNTs(I-III)-PEI-phage composites through CV and DPV-based current response. (A–C) CVs of BC-based composites with varying concentration of c-MWCNTs, including (A) 0.1 wt% c-MWCNTs, (B) 0.5 wt% c-MWCNTs, and (C) 1 wt% c-MWCNTs; and (D–F) DPVs of the BC-based composites with varying concentration of c-MWCNTs including (D) 0.1 wt% c-MWCNTs, (E) 0.5 wt% c-MWCNTs, and (F) 1 wt% c-MWCNTs.

between the BC/c-MWCNTs-PEI-phage surface and the solution. These observations are in accordance with previously reported studies (Wang et al., 2015; Yoon et al., 2006; Zhou et al., 2017). The immobilization of phage particles lowers the redox potential of the surrounding medium (Bhardwaj et al., 2016; Han et al., 2018; Shabani et al., 2009; Wang et al., 2018), which further explains the electron/charge flow characteristics of the BC/c-MWCNTs-PEI-phage electrode. Further, the results showed that BC/c-MWCNTs(II)-PEI-phage was the most efficient composite (Fig. 4B) based on the maximum increase in current response after phage immobilization. The impregnation of 1 wt% c-MWCNTs into BC showed an elevated current response followed by the PEI-modified BC composite, while only slight current variation was observed after phage immobilization (Fig. 4C). In contrast, the CV curve of 0.1 wt% c-MWCNTs showed a little current response variation as compared to 0.5 and 1 wt% c-MWCNTs, followed by an increase in current response with PEI-modified BC composite (Fig. 4A). The DPV results shown in Fig. 4D–F are in good agreement with CV curves of different BC-based composite films. The results showed that irrespective of different concentrations of c-MWCNTs (0.1, 0.5, and 1 wt%), an increase in current was observed with the polymerization of PEI and further upon the phage immobilization. Like CV curves, the DPV results also revealed that the composite with 0.5 wt% c-MWCNTs remained the most efficient electrode (Fig. 4E) as compared to other electrodes containing 0.1 wt% or 1 wt% c-MWCNTs (Fig. 4D and F). Therefore, the BC/c-MWCNTs (II)-PEI-phage composite was selected in the following experiments based on the maximum current response and comparatively high current response after phage immobilization as compared to BC/c-MWCNTs (I)-PEI-phage and BC/c-MWCNTs(III)-PEI-phage composites.

3.6. Electrochemical DPV-based S. aureus detection

3.6.1. Optimization and efficiency of BC/c-MWCNTs-PEI-phage biosensor

The DPV-based current response was used for the optimization of BC/phage-based biosensor and detection of *S. aureus*. The common factors like incubation time and pH generally affect the infection ability of phage, and ultimately the output of a biosensor. Therefore, it is essential to optimize the sensing conditions for improved sensitivity of the developed biosensor. First, the response time of the BC/c-MWCNTs-PEI-phage electrode was optimized by incubating the BC/phage-based electrode in PBS containing *S. aureus*. In parallel, DPV reading of PBS in the absence of *S. aureus* was used as a reference, and the electrode signal to bacterial cell density was compared. The results showed an identical signal to control after 10 min, while a decrease in current response was observed after 15 and 20 min (Fig. 5A). This decrease in the current response could be due to the deposition of *S. aureus* on the surface of electrode due to phage capturing, thus blocking the electron transfer (Mejri et al., 2010; Shabani et al., 2013; Wang et al., 2017; Zhou et al., 2017). At 25 min, a small increase in current response was observed, which could be due to bacterial cell lysis and release of the intracellular ions and progeny phages. Furthermore, as a result of cell lysis, the captured bacteria on the electrode surface can no more block the electron transfer. These results are in agreement with earlier reported studies (Mejri et al., 2010; Wang et al., 2015; Yoon et al., 2006; Zhou et al., 2017). The optimal time for phage activity was recorded to be 30 min, where a relatively considerable increase in current response was observed as compared to the slight increase in current response at 25 min and beyond 30 min (i.e., at 35, and 40 min) (Fig. 5A). These results are in accordance with previous reports, which also report an increase in current due to lysis of captured bacteria and subsequent release of cellular components and progeny phages (Bhardwaj et al., 2017a; Wang et al., 2017; Zhou et al., 2017). As reported earlier, phage particles reduce the redox potential of the surrounding medium (Bhardwaj et al., 2016; Han et al., 2018; Shabani et al., 2009; Wang et al., 2018), which further explains the electron/charge flow characteristics of the medium as well as electrode. Although the results show a gradual increase in the current response even between 30 and 45 min, this increase in current response was relatively low as compared to that at 30 min. It is understandable that all immobilized phages will not capture bacterial cells at the same time, some phages may involve in earlier while others in late bacterial capturing, thus current response time ranges between 25 and 45 min. The current response level-off between 50 and 60 min, which could be attributed to the lysis of all bacterial cells and release of progeny phages (Bhardwaj et al., 2017a; Wang et al., 2017; Zhou et al., 2017). The DPV-based current response curves concerning the incubation time are presented in Fig. S5A.

In general, phages usually show their activity at a wide pH range (4–10) (Wang et al., 2017; Wang et al., 2016b), indicating that performance of biosensors is pH-dependent. The developed BC/c-MWCNTs-PEI-phage electrode was incubated in PBS solution inoculated with *S. aureus* for 30 min (as optimized earlier) at varying pH between 4 and 10. The current response values were recorded for each solution to optimize the pH-dependent performance of biosensor. The results showed that the maximum current response was obtained at pH 7 (Fig. 5B), which is incomparable with the pH of optimum physical stability and lytic activity of phages (Wang et al., 2016b). The current response curves with respect to the varying pH are presented in Fig. S5B. Further, a gradual decrease in current response was observed at pH above and below neutral value, i.e., towards pH 4 and 10 (Fig. 5B). These results demonstrate that the developed biosensor can work at varying pH between 4 and 10 and best at neutral pH.

After optimizing the response time and pH-based performance of biosensor, the developed BC/c-MWCNTs-PEI-phage-based biosensor was employed for the detection of *S. aureus* in PBS at the optimal response time (i.e., 30 min) and pH (i.e., 7). The results in Fig. 5C shows that the current response was increased from control (PBS) along with the bacterial concentration from 3×10^0 to 3×10^7 CFU·mL^{-1}. This increase in current response could be attributed to the lysis of *S. aureus* caused by the immobilized phages and the subsequent release of intracellular components and progeny phages (Bhardwaj et al., 2017a; Wang et al., 2017; Zhou et al., 2017). The released intracellular components increase the conductivity of the medium, which in turn accounts for the high electron-transfer at the electrode-solution interface (Shabani et al., 2013; Zhou et al., 2017), while the released progeny phages further contribute to the infection of surrounding *S. aureus* cells. Such a chain of events, in the form of cell lysate, encourages the release of more intracellular components, which in turn further increase the electron transfer at the interface of solution-electrode (Shabani et al., 2009; Zhou et al., 2017), thus generating a stronger signal. A linear correlation in the current response was observed along with the log 10^0–10^7 CFU·mL^{-1} of *S. aureus* in PBS (Fig. 5D). The density of *S. aureus* in PBS was determined using the linear regression equation, where I (μA) = −1.011 log (CFU)-18.59 (R^2 = 0.989). The detection limit of *S. aureus* was calculated from the slope of the calibration curve using the below equation (Zhou et al., 2017):

$$\mathrm{LOD} = \frac{3\sigma}{\mathrm{m}} \quad (1)$$

where 'σ' represents the standard deviation of the blank and 'm' is the slope of the calibration curve. The standard deviation of blank PBS was 0.933, while the slope in the calibration curves was 1.011. The detection limit of the developed biosensor was calculated to be 3 CFU·mL^{-1}, while the linear range of detection was 10^0–10^7 CFU·mL^{-1} in 10 mL of PBS.

3.6.2. Specificity and stability of biosensor

The ability of the developed BC/c-MWCNTS-PEI-phage-based biosensor to detect the specific bacteria was determined in the presence of different non-specific bacteria, as well in a mixture of phage-specific host and non-host bacteria. The results showed a negligible current response for non-specific bacteria as compared to the control (Fig. 5E), and the respective DPV-based current response variations are presented in Fig. S5C. In contrast, the culture of pure *S. aureus*, as well as

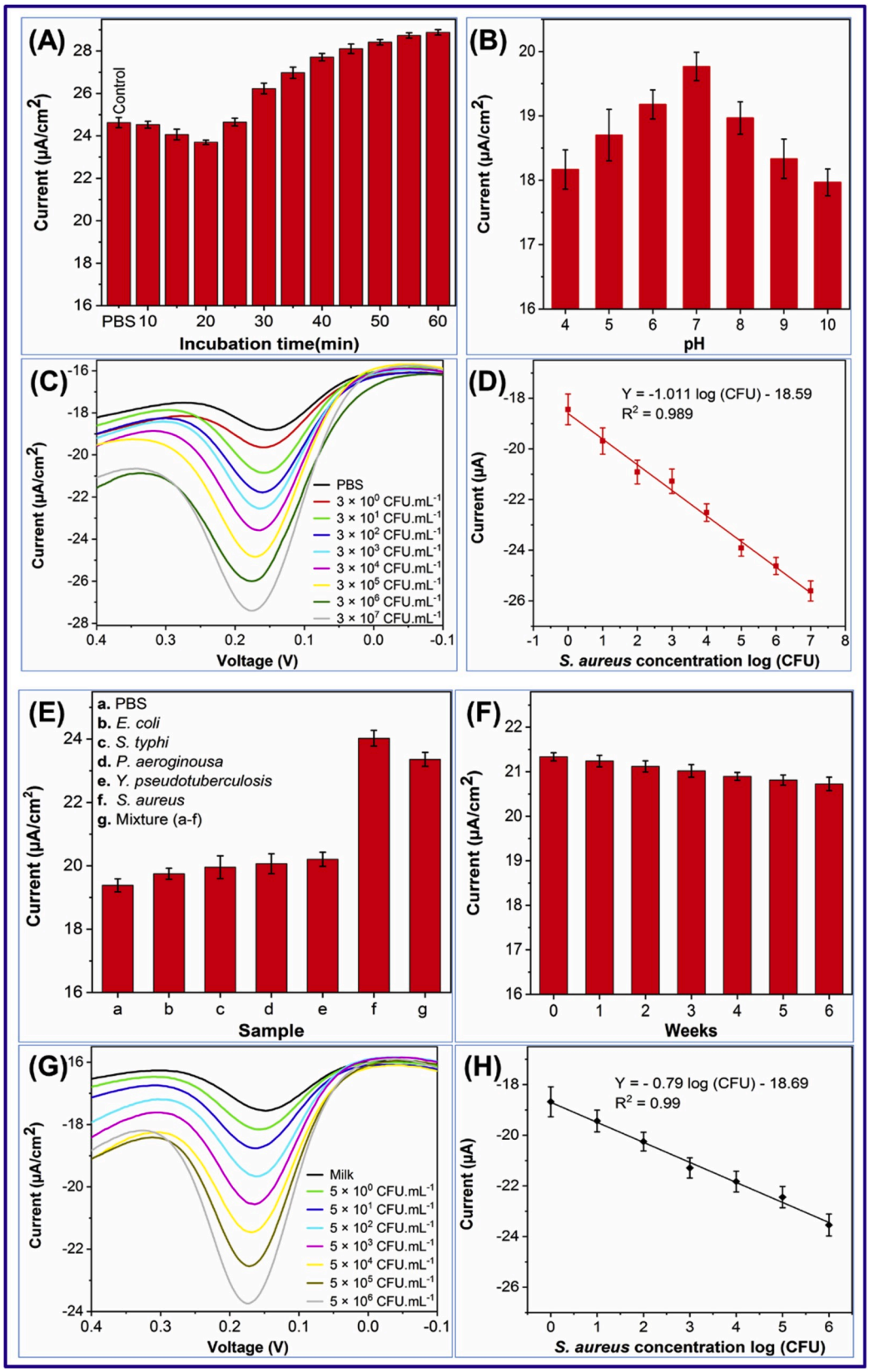

Fig. 5. Optimization, specificity, and stability of BC/c-MWCNTs-PEI-phage biosensor and its application for *S. aureus* detection in PBS and milk. (A) The response time concerning the net increase in current response and (B) the effect of pH on the current response. (C) The DPV curves of detected *S. aureus* concentrations in PBS, (D) linear range of log *S. aureus* detected in PBS, (E) specificity of the biosensor to detect *S. aureus* with respect to non-target bacteria, (F) stability of electrode stored at 4 °C, over 6 weeks, (G) DPV curves of detected *S. aureus* concentrations in the milk sample, and (H) linear range of log *S. aureus* in the milk sample. The standard deviations of triplicate measurements are indicated by error bars, analyzed by Origin Pro. Software.

the mixture of host and non-host bacteria, showed significant current response variations. These results demonstrate that the developed biosensor could specifically detect *S. aureus*, even in the presence of non-host bacteria.

The stability of the developed BC/c-MWCNTs-PEI-phage biosensor was determined by storing it at 4 °C. The stability assay demonstrated no obvious current response changes against ~10^6 CFU·mL^{-1} of *S. aureus* (Fig. 5F). The biosensor showed good stability: with relative standard deviation (RSD) of 0.0907 and 0.152 and mean current of 21.33 and 20.73 μA·cm^{-2} at zero weeks and after six-weeks, respectively. The DPV-based current response variations are presented in Fig. S5D. These results indicate that the developed biosensor could be used for an extended period and can be easily moved to a new place. This high stability of biosensor could be attributed to the never-dried nature of BC (Yoon et al., 2006) that provides a humid environment to the immobilized phages.

3.6.3. Real food sample analysis and accuracy of biosensor

A biosensor is considered practical if it can detect the target analyte in real samples (Bhardwaj et al., 2016); therefore, the performance of the developed BC/c-MWCNTs-PEI-phage biosensor was evaluated for detection of *S. aureus* in milk. The biosensor effectively detected *S. aureus* in milk, as indicated by an increase in current response with the increasing bacterial cell density (Fig. 5G). These results demonstrate the sensing efficiency of the developed biosensor to detect *S. aureus* in real food samples, although the current response in PBS was slightly higher as compared to the milk due to its complex nature, as shown in Fig. 5C and G, respectively. Further, the working concentration range of detection after 30 min of incubation was found to be between 5 × 10^0 and 5 × 10^6 CFU·mL^{-1} in milk. As demonstrated in Fig. 5C and G, the biosensor effectively detected up to 3 × 10^7 and 5 × 10^6 CFU·mL^{-1} both in PBS and milk, respectively. Likewise PBS, a linear correlation in the current response was observed in milk along with the log 10^0–10^6 CFU·mL^{-1} of *S. aureus* (Fig. 5H). The density of *S. aureus* was determined in the milk by using linear regression equation (1), where I (μA) = −0.79 log (CFU)-18.69 (R^2 = 0.99), while the detection limit was determined using equation (1) as stated for PBS. For blank milk, the standard deviation was found to be 1.289, while the slope in the calibration curve was 0.79. The detection limit was calculated to be 5 CFU·mL^{-1}, while the linear range of detection was 10^0–10^6 CFU·mL^{-1} in 10 mL of milk sample.

The accuracy of the developed biosensor was evaluated by quantifying the number of *S. aureus* cells inoculated in PBS and milk samples, both by the biosensor and the conventional culturing and plate count methods. PBS and milk samples with known amount *S. aureus*, i.e., 3 × 10^3 and 5.2 × 10^3 CFU·mL^{-1}, respectively, were prepared and the accuracy of the developed biosensor was assessed by comparing the % recovery of the biosensor with the plate count method (Table S2), which showed comparable results (Fig. S6). These results suggest that the developed biosensor is accurate and acceptable; this can be used for the detection and quantification of *S. aureus* in real samples. Furthermore, the ability of the developed biosensor to discriminate live bacterial cells in a mixture of live/dead cells was evaluated by analyzing the DPV-based current response in cultures of live, dead, and mixture of live/dead cells. The results showed an overlapped current response of dead cells with the control (i.e., PBS). In contrast, the live cells and mixture of live/dead cells showed obvious current responses, demonstrating the ability of biosensor to discriminate live bacterial cells in a mixture of live/dead cells (Fig. S7). A comparison of the results of the developed BC/c-MWCNTs-PEI-phage electrochemical biosensor in the present study with the previously reported most recent and significant reports for *S. aureus* detection is presented in Table 1. In addition, the developed biosensor remained highly sensitive, stable, selective, and was able to discriminate live bacterial cells in a mixture of live/dead cells.

4. Conclusions

The present study is the first report of the immobilization of phages in bacterial cellulose for electrochemical detection of bacteria. Functionalization of the developed BC/c-MWCNTs nanocomposite with PEI (a poly-cation) facilitated active immobilization of phage particles in a 'head-down and tail-up' orientation at a high density. This orientation of the developed bio-nanomaterial as a transducer offered active and high density of phage particles immobilization (11.7 ± 1.2 phage particles·μm^{-2}), which in turn resulted in improved sensitivity of the biosensor. The developed biosensor effectively detected 3 and 5 CFU·mL^{-1} of *S. aureus* in PBS and milk sample, respectively, within 30 min with high sensitivity, specificity, and accuracy. The biosensor performed well at a broad pH-range between 4 and 10, with maximum sensitivity at neutral pH. The developed biosensor was stable over 6 weeks at 4 °C and effectively discriminated live bacterial cells in a mixture of live/dead cells. The performance of the developed biosensor can be further improved by optimizing the phage concentration and the deposition time, while the approach can be extended for the on-site detection of *S. aureus*, specifically in food samples.

Declaration of competing interest

The authors declare that they have no known competing financial interests or personal relationships that could have appeared to influence the work reported in this paper.

Table 1
Performance comparison of BC/c-MWCNTs-PEI-phage biosensor with most recently reported significant biosensors for *S. aureus* detection.

Substrate	Bioprobe	Assay type	Detection range (CFU·mL^{-1})	Assay time (min)	LOD (CFU·mL^{-1})	Sample	Live/dead cells discrimination	Ref.
rGO-AuNP/GCE	Aptamer	Impedimetric	10–10^6	60	10	Culture	No	Jia et al., (2014)
Gold electrode	Antibody	Impedimetric	10^1–10^7	30	10	Culture	No	Bekir et al., (2015)
Gold nanoparticle	Enzyme	DPV	–	<60	10^2	Water	No	Chen et al., (2015)
SWCNTs	Antibody	Conductometric	10^3–10^9	–	10	Culture	No	Yoo et al., (2016)
SWCNTs/SPE	Antibody	DPV, CV	10–10^7	30	13	Milk	No	Bhardwaj et al. (2017a))
MOF based on NH_2-MIL-53	Phage	Photo-luminescence	40–4 × 10^8	–	31	Pastry cream	–	Bhardwaj et al. (2017b))
BC/MWCNTs-PEI	Phage	DPV	3 × 10^0–3 × 10^7	30	3	PBS	Yes	Current work
			5 × 10^0–5 × 10^6		5	Milk		

rGO = Reduced graphene oxide; AuNPs = Gold nanoparticles; GCE = Glassy carbon electrode; SWCNTs = Single walled carbon nanotubes; SPE = Screen printed electrode.

CRediT authorship contribution statement

Umer Farooq: Conceptualization, Methodology, Software, Writing - original draft. **Muhammad Wajid Ullah:** Conceptualization, Methodology, Software, Writing - original draft. **Qiaoli Yang:** Data curation. **Ayesha Aziz:** Visualization, Investigation. **Jingjing Xu:** Software, Validation. **Lei Zhou:** Supervision. **Shenqi Wang:** Funding acquisition, Project administration, Supervision, Writing - review & editing.

Acknowledgment

This work was supported by the National Key Research and Development Program of China under Grant 2017YFC1104402, China Postdoctoral Science Foundation (2016M602291), the initial Research fund from the Chinese Scholarship Council (CSC); and 3551 Project, Optics Valley of China.

Appendix A. Supplementary data

Supplementary data to this article can be found online at https://doi.org/10.1016/j.bios.2020.112163.

References

Anany, H., Chen, W., Pelton, R., Griffiths, M.W., 2011. Appl. Environ. Microbiol. 77, 6379–6387. https://doi.org/10.1128/AEM.05493-11.
Archer, M.J., Liu, J.L., 2009. Sensors 9, 6298–6311. https://doi.org/10.3390/s90806298.
Arora, P., Sindhu, A., Dilbaghi, N., Chaudhury, A., 2011. Biosens. Bioelectron. 28, 1–12. https://doi.org/10.1016/j.bios.2011.06.002.
Asif, M., Aziz, A., Azeem, M., Wang, Z., Ashraf, G., Xiao, F., Chen, X., Liu, H., 2018. Adv. Colloid Interface Sci. 262, 21–38. https://doi.org/10.1016/j.cis.2018.11.001.
Balasubramanian, S., Sorokulova, I.B., Vodyanoy, V.J., Simonian, A.L., 2007. Biosens. Bioelectron. 22, 948–955. https://doi.org/10.1016/j.bios.2006.04.003.
Bekir, K., Barhoumi, H., Braiek, M., Chrouda, A., Zine, N., Abid, N., Maaref, A., Bakhrouf, A., Ouada, H. Ben, Jaffrezic-Renault, N., Mansour, H. Ben, 2015. Environ. Sci. Pollut. Res. 22, 15796–15803. https://doi.org/10.1007/s11356-015-4761-7.
Bhardwaj, J., Devarakonda, S., Kumar, S., Jang, J., 2017a. Sensor. Actuator. B Chem. 253, 115–123. https://doi.org/10.1016/j.snb.2017.06.108.
Bhardwaj, N., Bhardwaj, S.K., Mehta, J., Kim, K.-H., Deep, A., 2017b. ACS Appl. Mater. Interfaces 9, 33589–33598. https://doi.org/10.1021/acsami.7b07818.
Bhardwaj, N., Bhardwaj, S.K., Mehta, J., Mohanta, G.C., Deep, A., 2016. Anal. Biochem. 505, 18–25. https://doi.org/10.1016/j.ab.2016.04.008.
Chen, J., Jiang, Z., Ackerman, J.D., Yazdani, M., Hou, S., Nugen, S.R., Rotello, V.M., 2015. Analyst 140, 4991–4996. https://doi.org/10.1039/c5an00637f.
Chen, P., Kim, H.S., Kwon, S.M., Yun, Y.S., Jin, H.J., 2009. Curr. Appl. Phys. 9, e96–e99. https://doi.org/10.1016/j.cap.2008.12.038.
Czaja, W., Krystynowicz, A., Bielecki, S., Brown, R.M., 2006. Biomaterials 27, 145–151. https://doi.org/10.1016/j.biomaterials.2005.07.035.
Dong, D., Zhang, Y., Sutaria, S., Konarov, A., Chen, P., 2013. PLoS One 8, e82332. https://doi.org/10.1371/journal.pone.0082332.
Farooq, U., Yang, Q., Ullah, M.W., Wang, S., 2018. Biosens. Bioelectron. 118, 204–216. https://doi.org/10.1016/j.bios.2018.07.058.
Geisel, N., Clasohm, J., Shi, X., Lamboni, L., Yang, J., Mattern, K., Yang, G., Schäfer, K.H., Saumer, M., 2016. Small 12, 5407–5413. https://doi.org/10.1002/smll.201601679.
Goeller, L.J., Riley, M.R., 2007. Appl. Spectrosc. 61, 679–685. https://doi.org/10.1366/000370207781393217.
Guo, Q., Han, J.J., Shan, S., Liu, D.F., Wu, S.S., Xiong, Y.H., Lai, W.H., 2016. Biosens. Bioelectron. 86, 990–995. https://doi.org/10.1016/j.bios.2016.07.049.
Han, L., Xia, H., Yin, L., Petrenko, V.A., Liu, A., 2018. Biosens. Bioelectron. 106, 1–6. https://doi.org/10.1016/j.bios.2018.01.046.
Hosseinidoust, Z., Olsson, A.L.J., Tufenkji, N., 2014. Colloids Surf. B Biointerfaces 124, 2–16. https://doi.org/10.1016/j.colsurfb.2014.05.036.
Huang, Q., Zhao, J., Liu, M., Chen, J., Zhu, X., Wu, T., Tian, J., Wen, Y., Zhang, X., Wei, Y., 2018. J. Taiwan Inst. Chem. Eng. 82, 92–101. https://doi.org/10.1016/j.jtice.2017.10.019.
Janczuk-Richter, M., Marinović, I., Niedziółka-Jönsson, J., Szot-Karpińska, K., 2019. Electrochem. Commun. 99, 11–15. https://doi.org/10.1016/j.elecom.2018.12.011.
Janczuk, M., Richter, Ł., Hoser, G., Kawiak, J., Łoś, M., Niedziółka-Jönsson, J., Paczesny, J., Hołyst, R., 2017. Bioconjugate Chem. 28, 419–425. https://doi.org/10.1021/acs.bioconjchem.6b00596.
Järvinen, A.K., Laakso, S., Piiparinen, P., Aittakorpi, A., Lindfors, M., Huopaniemi, L., Piiparinen, H., Mäki, M., 2009. BMC Microbiol. 9, 161. https://doi.org/10.1186/1471-2180-9-161.
Jarvis, R.M., Goodacre, R., 2004. Anal. Chem. 76, 40–47. https://doi.org/10.1021/ac034689c.
Jasim, A., Ullah, M.W., Shi, Z., Lin, X., Yang, G., 2017. Carbohydr. Polym. 163, 62–69. https://doi.org/10.1016/j.carbpol.2017.01.056.
Jia, F., Duan, N., Wu, S., Ma, X., Xia, Y., Wang, Z., Wei, X., 2014. Microchim. Acta 181, 967–974. https://doi.org/10.1007/s00604-014-1195-8.
Jin, X., Xiang, Z., Liu, Q., Chen, Y., Lu, F., 2017. Bioresour. Technol. 244, 844–849. https://doi.org/10.1016/j.biortech.2017.08.072.
Khan, S., Ul-Islam, M., Ikram, M., Islam, S.U., Ullah, M.W., Israr, M., Jang, J.H., Yoon, S., Park, J.K., 2018. Int. J. Biol. Macromol. 117, 1200–1210. https://doi.org/10.1016/j.ijbiomac.2018.06.044.
Khan, S., Ul-Islam, M., Khattak, W.A., Ullah, M.W., Park, J.K., 2015. Carbohydr. Polym. 127, 86–93. https://doi.org/10.1016/j.carbpol.2015.03.055.
Kumar, Suveen, Kumar, Saurabh, Tiwari, S., Augustine, S., Srivastava, S., Yadav, B.K., Malhotra, B.D., 2016. Sensor. Actuator. B Chem. 235, 1–10. https://doi.org/10.1016/j.snb.2016.05.047.
Lakshmanan, R.S., Guntupalli, R., Hu, J., Petrenko, V.A., Barbaree, J.M., Chin, B.A., 2007. Sensor. Actuator. B Chem. 126, 544–550. https://doi.org/10.1016/j.snb.2007.04.003.
Li, S., Jasim, A., Zhao, W., Fu, L., Ullah, M.W., Shi, Z., Yang, G., 2018a. ES Mater. Manuf. 1, 41–49. https://doi.org/10.30919/esmm5f120.
Li, Y., Xie, G., Qiu, J., Zhou, D., Gou, D., Tao, Y., Li, Yi, Chen, H., 2018b. Sensor. Actuator. B Chem. 258, 803–812. https://doi.org/10.1016/j.snb.2017.11.155.
Liana, A.E., Chia, E.W., Marquis, C.P., Gunawan, C., Gooding, J.J., Amal, R., 2016. J. Colloid Interface Sci. 468, 192–199. https://doi.org/10.1016/j.jcis.2016.01.052.
Lv, P., Feng, Q., Wang, Q., Li, D., Zhou, J., Wei, Q., 2016. Fibers Polym. 17, 1858–1865. https://doi.org/10.1007/s12221-016-6337-7.
Lv, P., Zhou, H., Mensah, A., Feng, Q., Wang, D., Hu, X., Cai, Y., Amerigo Lucia, L., Li, D., Wei, Q., 2018. Chem. Eng. J. 351, 177–188. https://doi.org/10.1016/j.cej.2018.06.098.
Maria Manzine Costa, L., Molina de Olyveira, G., Basmaji, P., Xavier Filho, L., 2012. J. Biomaterials Nanobiotechnol. 3, 92–96. https://doi.org/10.4236/jbnb.2012.31012.
Mejri, M.B., Baccar, H., Baldrich, E., Del Campo, F.J., Helali, S., Ktari, T., Simonian, A., Aouni, M., Abdelghani, A., 2010. Biosens. Bioelectron. 26, 1261–1267. https://doi.org/10.1016/j.bios.2010.06.054.
Moghtader, F., Congur, G., Zareie, H.M., Erdem, A., Piskin, E., 2016. RSC Adv. 6, 97832–97839. https://doi.org/10.1039/C6RA18884B.
Pallavali, R.R., Degati, V.L., Lomada, D., Reddy, M.C., Durbaka, V.R.P., 2017. PLoS One 12, e0179245. https://doi.org/10.1371/journal.pone.0179245.
Pourreza, N., Golmohammadi, H., Naghdi, T., Yousefi, H., 2015. Biosens. Bioelectron. 74, 353–359. https://doi.org/10.1016/j.bios.2015.06.041.
Preisner, O., Guiomar, R., Machado, J., Menezes, J.C., Lopes, J.A., 2010. Appl. Environ. Microbiol. 76, 3538–3544. https://doi.org/10.1128/AEM.01589-09.
Richter, Ł., Bielec, K., Leśniewski, A., Łoś, M., Paczesny, J., Hołyst, R., 2017. ACS Appl. Mater. Interfaces 9, 19622–19629. https://doi.org/10.1021/acsami.7b03497.
Scharff, R.L., 2012. J. Food Protect. 75, 123–131. https://doi.org/10.4315/0362-028X.JFP-11-058.
Shabani, A., Marquette, C.A., Mandeville, R., Lawrence, M.F., 2013. Talanta 116, 1047–1053. https://doi.org/10.1016/j.talanta.2013.07.078.
Shabani, A., Zourob, M., Allain, B., Mandeville, R., 2009. U.S. patent 20090068638 A1.
Singh, A., Glass, N., Tolba, M., Brovko, L., Griffiths, M., Evoy, S., 2009. Biosens. Bioelectron. 24, 3645–3651. https://doi.org/10.1016/j.bios.2009.05.028.
Singh, A., Poshtiban, S., Evoy, S., 2013. Sensors 13, 1763–1786. https://doi.org/10.3390/s130201763.
Szymańska-Chargot, M., Cybulska, J., Zdunek, A., 2011. Sensors 11, 5543–5560. https://doi.org/10.3390/s110605543.
Tolba, M., Minikh, O., Brovko, L.Y., Evoy, S., Griffiths, M.W., 2010. Appl. Environ. Microbiol. 76, 528–535. https://doi.org/10.1128/AEM.02294-09.
Ul-Islam, M., Khattak, W.A., Kang, M., Kim, S.M., Khan, T., Park, J.K., 2013. Cellulose 20, 253–263. https://doi.org/10.1007/s10570-012-9799-9.
Ul-Islam, M., Khattak, W.A., Ullah, M.W., Khan, S., Park, J.K., 2014. Cellulose 21, 433–447. https://doi.org/10.1007/s10570-013-0109-y.
Ul-Islam, M., Subhan, F., Islam, S.U., Khan, S., Shah, N., Manan, S., Ullah, M.W., Yang, G., 2019. Int. J. Biol. Macromol. 137, 1050–1059. https://doi.org/10.1016/j.ijbiomac.2019.07.050.
Ullah, M.W., Ul-Islam, M., Khan, S., Kim, Y., Jang, J.H., Park, J.K., 2016. RSC Adv. 6, 22424–22435. https://doi.org/10.1039/c5ra26704h.
Ullah, M.W., Ul-Islam, M., Khan, S., Kim, Y., Park, J.K., 2015. Carbohydr. Polym. 132, 286–294. https://doi.org/10.1016/j.carbpol.2015.06.037.
Ullah, M.W., Ul Islam, M., Khan, S., Shah, N., Park, J.K., 2017. Kor. J. Chem. Eng. 34, 1591–1599. https://doi.org/10.1007/s11814-017-0121-2.
Wang, C., Sauvageau, D., Elias, A., 2016a. ACS Appl. Mater. Interfaces 8, 1128–1138. https://doi.org/10.1021/acsami.5b08664.
Wang, D., Chen, J., Nugen, S.R., 2017. Anal. Chem. 89, 1650–1657. https://doi.org/10.1021/acs.analchem.6b03752.
Wang, D., Hinkley, T., Chen, J., Talbert, J.N., Nugen, S.R., 2018. Analyst 144, 1345–1352. https://doi.org/10.1039/c8an01850b.
Wang, J., Lu, X., Ng, P.F., Lee, K.I., Fei, B., Xin, J.H., Wu, J. yong, 2015. J. Colloid Interface Sci. 440, 32–38. https://doi.org/10.1016/j.jcis.2014.10.035.
Wang, Y., Ye, Z., Ying, Y., 2012. Sensors 12, 3449–3471. https://doi.org/10.3390/s120303449.
Wang, Z., Wang, D., Kinchla, A.J., Sela, D.A., Nugen, S.R., 2016b. Anal. Bioanal. Chem. 408, 4169–4178. https://doi.org/10.1007/s00216-016-9511-2.
Wu, L., Song, Y., Luan, T., Ma, L., Su, L., Wang, S., Yan, X., 2016. Biosens. Bioelectron. 86, 102–108. https://doi.org/10.1016/j.bios.2016.06.041.
Yemini, M., Levi, Y., Yagil, E., Rishpon, J., 2007. Bioelectrochemistry 70, 180–184. https://doi.org/10.1016/j.bioelechem.2006.03.014.
Yoo, S.M., Baek, Y.-K., Shin, S.H.R., Kim, J.-H., Jung, H.-T., Choi, Y.-K., Lee, S.Y., 2016. J. Nanosci. Nanotechnol. 16, 6520–6525. https://doi.org/10.1166/jnn.2016.10882.

Yoon, S.H., Jin, H.J., Kook, M.C., Pyun, Y.R., 2006. Biomacromolecules 7, 1280–1284. https://doi.org/10.1021/bm050597g.
Yuan, J., Wu, S., Duan, N., Ma, X., Xia, Y., Chen, J., Ding, Z., Wang, Z., 2014. Talanta 127, 163–168. https://doi.org/10.1016/j.talanta.2014.04.013.
Yue, H., He, Y., Fan, E., Wang, L., Lu, S., Fu, Z., 2017. Biosens. Bioelectron. 94, 429–432. https://doi.org/10.1016/j.bios.2017.03.033.
Yue, Y., Han, J., Han, G., Zhang, Q., French, A.D., Wu, Q., 2015. Carbohydr. Polym. 133, 438–447. https://doi.org/10.1016/J.CARBPOL.2015.07.058.
Zhang, T., Wang, W., Zhang, D., Zhang, X., Yurong, M., Zhou, Y., Qi, L., 2010. Adv. Funct. Mater. 20, 1152–1160. https://doi.org/10.1002/adfm.200902104.
Zhao, X., Lin, C.W., Wang, J., Oh, D.H., 2014. J. Microbiol. Biotechnol. 24, 297–312. https://doi.org/10.4014/jmb.1310.10013.
Zhou, Y., Marar, A., Kner, P., Ramasamy, R.P., 2017. Anal. Chem. 89, 5734–5741. https://doi.org/10.1021/acs.analchem.6b03751.